ACCSCIENCE PUBLISHING

International Journal of Bioprinting

RESEARCH ARTICLE

Replication of an intervertebral disc using an in-house bioprinter: A proof-of-concept study

Emmaëlle Carrot[1], Perrine de Villemagne[2], Paul Humbert[1], Sébastien Grastilleur[1], Benoit Rosa[2], Boris Halgand[1], Yoan Le Guennec[1], Johann Clouet[1], Vianney Delplace[1], Pierre Weiss[1], Franck Halary[3], Jean-Yves Hascoët[2], Marion Fusellier[1], Luciano Vidal[2,4], Jérôme Guicheux[1]*, and Catherine Le Visage[1]*

[1]Nantes Université, Oniris, INSERM, CHU Nantes, Regenerative Medicine and Skeleton, RMeS, UMR 1229, Nantes, Pays de la Loire, France

[2]CNRS UMR 6183, Nantes Université, École Centrale Nantes, Rapid Manufacturing Platform, Institut de Recherche en Génie Civil et Mécanique (GeM), Nantes, Pays de la Loire, France

[3]3Nantes Université, INSERM, Center for Research in Transplantation and Translational Immunology, UMR 1064, Nantes, Pays de la Loire, France

[4]Department of Plastic and Reconstructive Surgery, Clinique Bretéché - ELSAN, Nantes, Pays de la Loire, France

(This article belongs to the Special Issue: *Advances in Bioprinting and Organ-on-a-chip and Applications for Precision Medicine*)

Abstract

The intervertebral disc, a fibro-cartilaginous structure, contains a gelatinous core (*nucleus pulposus*) surrounded by collagen fiber lamellae (*annulus fibrosus*). Intervertebral disc degeneration leads to a debilitating disorder, and new treatments are currently being developed. Unfortunately, conventional monolayer *in vitro* models fail to predict the clinical efficacy of novel therapies accurately. Here, we report a bioprinted construct that mimics the macroscopic and microscopic architecture of the intervertebral disc. First, a 3D model was created from a histological section of a sheep lumbar intervertebral disc. The printability of the ink, gelatin (7% w/v), alginate (0.6% w/v), and hyaluronic acid (0.2% w/v) was optimized by varying the printing pressure (70–110 kPa), printing speed (2–10 mm/s), and nozzle type (needle or tip). *Nucleus pulposus* and *annulus fibrosus* cells, harvested from 4-month-old lambs, were bioprinted (5×10^5 cells/mL) using an in-house extrusion bioprinter. Cell viability (live/dead assay), shape (actin immunostaining), distribution (confocal microscopy), and matrix synthesis (immunostaining) were evaluated after 21 days of culture. We used a parametric study to quantify and optimize the factors (pressure, printing speed, nozzle type) influencing the filament width. The 3D construct exhibited fidelity to the initial design and maintained stability in length, width, and height for 21 days. Fluorescent labeling confirmed the distribution of *nucleus pulposus* and *annulus fibrosus* cells in each tissue, replicating the native intervertebral disc structure. We also evidenced cell viability and collagen type 1 synthesis. This bioprinted construct offers a promising alternative to current *in vitro* models, potentially enabling more relevant preclinical evaluations.

Keywords: 3D bioprinting; Alginate; Hydrogel; In-house extrusion bioprinter; *In vitro* 3D model; Gelatin; Hyaluronic acid

***Corresponding authors:**
Catherine Le Visage (catherine.levisage@inserm.fr)

Jérôme Guicheux (jerome.guicheux@univ-nantes.fr)

Citation: Carrot E, de Villemagne P, Humbert P, et al. Replication of an intervertebral disc using an in-house bioprinter: A proof-of-concept study. *Int J Bioprint.* 2025;11(1):470-484. doi: 10.36922/ijb.5021

Received: October 10, 2024
1st revised: November 12, 2024
2nd revised: December 1, 2024
3rd revised: December 6, 2024
Accepted: December 9, 2024
Published Online: December 9, 2024

Copyright: © 2024 Author(s). This is an Open Access article distributed under the terms of the Creative Commons Attribution License, permitting distribution, and reproduction in any medium, provided the original work is properly cited.

Publisher's Note: AccScience Publishing remains neutral with regard to jurisdictional claims in published maps and institutional affiliations.

1. Introduction

The intervertebral disc (IVD) is a fibro-cartilaginous structure essential for maintaining the mobility and stability of the human spine and absorbing and distributing shocks.[1,2] It consists of three primary tissues: a central gelatinous core (*nucleus pulposus* [NP]), an outer network of collagen fibers (*annulus fibrosus* [AF]), and two cartilaginous endplates on either side, which connect to the vertebral bodies.[3,4] The NP is a highly hydrated tissue comprising 70%–90% of water[5] bound by sulfate proteoglycans[6,7] and randomly organized type II collagen fibers,[8,9] with a viscoelastic behavior.[10–12] The young and healthy NP contains two cell types: large notochordal cells, whose number decreases with age,[13] marking the onset of disc degeneration,[14] and nucleopulpocytes or NP cells, resembling articular chondrocytes.[15,16] The total cell density in the NP is about 4200 cells/mm^3[3,17] and both cells are responsible for maintaining homeostasis by synthesizing the extracellular matrix (ECM).[18] The NP is surrounded by the AF, which consists of 15–25 concentric fibrocartilaginous lamellar bands of type I collagen fibers.[19,20] The AF structure is highly resistant, retaining the NP during spinal movements.[21,22] The AF cells, located between the lamellae and aligned with the collagen fibers, are fibroblast-like cells with an elongated shape and produce their surrounding ECM.[23] In young and healthy AF, cells are found at a density of about 12,000 cells/mm^3, and this number tends to decrease with age.[24]

Due to the high frequency of movement, IVD is frequently disrupted, causing degenerative changes.[25] This degeneration is responsible for 40% of low back pain cases,[26] which affects 80% of the global population at least once in their lifetime.[27] The etiology of IVD degeneration remains poorly understood, and existing treatments, such as spinal fusion or IVD replacement, fail to maintain the IVD tissue integrity or halt its decline.[28] In the long term, these surgical interventions may even accelerate the process of IVD degeneration. Presently, novel therapies are being developed to address the etiological cause of degeneration. These new treatments include gene therapy[29] and cell therapy,[30] often combined with the injection of a biomaterial.[31] Each of these therapies acts on one or several aspects of the degeneration. An ECM-mimicking biomaterial can directly restore mechanical properties,[32] and injection of growth factors[33] or gene therapy[34] can stimulate ECM synthesis, relieve inflammation,[35,36] and delay disease progression. The evaluation of these therapies mainly relies on 2D *in vitro* models before progressing to *in vivo* models.[37] Despite the widespread use of 2D *in vitro* culture models, their lack of morphological complexity and cell–ECM interactions significantly oversimplifies the cellular environment. 3D *in vitro* culture systems, such as pellet configuration[38] or encapsulation in alginate hydrogel,[39] have been explored to maintain IVD cell phenotype as seen in native conditions. Although these 3D models are more relevant as they replicate the 3D IVD structure, they are limited to one tissue, AF or NP, and lack repeatability and reproducibility.[40] Only a few complete models replicating the 3D structure of the disc, along with its particular tissues, have been documented.[41] These artificial IVD models were developed for total disc replacement and demonstrated a partial restoration of the spine biomechanics.[42,43] However, the design of these models was not intended to evaluate biological treatments, as the maturation of the model occurs *in vivo* to reproduce a healthy IVD.

Therefore, in this study, we aim to develop a 3D construct that mimics an ovine IVD from a macroscopic and microscopic point of view, with *in vitro* maturation, so that this model could be used to evaluate new therapeutic strategies. The ovine spine is primarily used as a preclinical model because of its biomechanical and cellular similarities with the human one.[44] A bioprinting technique was used to reproduce the specific shape of the IVD and deposit the cells constituting the model. We specially designed an in-house 3D extrusion bioprinter for this project. The bioprinting path was adapted from the histological section of sheep lumbar IVD to be as close to native tissue as possible. Cells extracted from young lumbar ovine IVDs were encapsulated into a gelatin/alginate/hyaluronic acid (HA) ink. This ink was designed to provide the cells with a favorable 3D environment, enabling them to secrete *de novo* ECM, which, after maturation, will form an IVD-like tissue.[45] After optimizing the bioprinting parameters, constructs were obtained and evaluated for up to 21 days of culture. We demonstrated that cells were well homogeneously distributed into the IVD construct and remained viable for up to 21 days of culture. Moreover, both cells in the IVD exhibited a round shape and synthesized collagen, a major component of the IVD ECM.

2. Materials and methods

2.1. Bioprinter

For the development of the bioprinter, a set of specifications was considered based on the type of bioinks to be used and the type of structure to be printed. Temperature control at the level of the printing head and the printing plate was conceived. Separate control of both was designed, with a temperature range between -25 and 100°C. A laser control system was mounted on the deposition plate to position and control the printing head on the printer plate and its different axes. Three linear axes were composed by an encoder resolution of 0.01 µm, ±0.4 µm of bidirectional repeatability, and ±2.5 µm positional accuracy. A post-

processing system was meticulously developed to correct and control the printer's trajectories, ensuring the high quality of the printed objects designed and conceived using computer-aided design (CAD) (Figure 1).

2.2. Optimization of the ink formulation

Different concentrations (w/v) of alginate from brown algae (A2033; Sigma Aldrich, USA), gelatin from bovine skin (G9391; Sigma Aldrich, USA), and HA from *Streptococcus* (53747; Sigma Aldrich, USA) were tested (Table 1). Formulations 1–3 contain 0.6%, 1.2%, or 1.8% of alginate, respectively, 8% of gelatin, and no HA. In formulations 4–9, gelatin was set to 7%, and alginate was set at 0.6% or 1.2% for formulations 4–6 and 7–9, respectively. HA concentration was set at 0% for formulations 4 and 6, 0.2% for formulations 5–8, and 0.3% for formulations 6 and 9.

The powders were mixed in warm water (30–50°C) to solubilize the gelatin. The desired ink volume was transferred into a 10 mL syringe (7012112; Nordson, USA). A plunger sealed the syringe (7012178; Nordson, USA). Air bubbles were removed by centrifugation at 260 × *g* for 3 min. The ink was then equilibrated at 22°C to induce a pre-gelation step, making it printable. Inks were placed into the bioprinter developed by Ecole Centrale Nantes (France) and extruded through different needle diameters (0.20 and 0.25 mm) at 20 kPa and with a printing speed of 10 mm/s to form a square of 1 × 1 cm on 10 layers. Parameters based on the ink aspect (granular or homogeneous), the extrusion process (continuous or not), and the filament uniformity (ranging from + [irregular] to +++ [uniform]) were visually assessed to validate the ink formulation.

2.3. Optimization of printing parameters

After selecting the ink formulation, the printing parameters were defined. The influence of the nozzle type, the extrusion pressure, and the printing speed were assessed to optimize the printing resolution. Two nozzle types were tested: a 0.20 or 0.25 mm internal diameter stainless steel needle and a 0.20 or 0.25 mm internal diameter polyethylene tip. The printing speed was set at 4, 8, or 10 mm/s, and the extrusion pressure was set at 70, 90, or 110 kPa. For each condition, two 2-cm-long filaments were extruded and photographed, and four measurements of the filament thickness were performed. The cordon width was measured using ImageJ® software (1.54j; National Institutes of Health, United States of America [USA]). The optimal printing parameters were selected to obtain the finest filament for greater printing precision (n = 3 independent experiments).

2.4. Cell isolation and culture

Two 4-month-old lambs from Ecole Nationale Vétérinaire de Nantes (ONIRIS) were used to collect NP and AF cells.

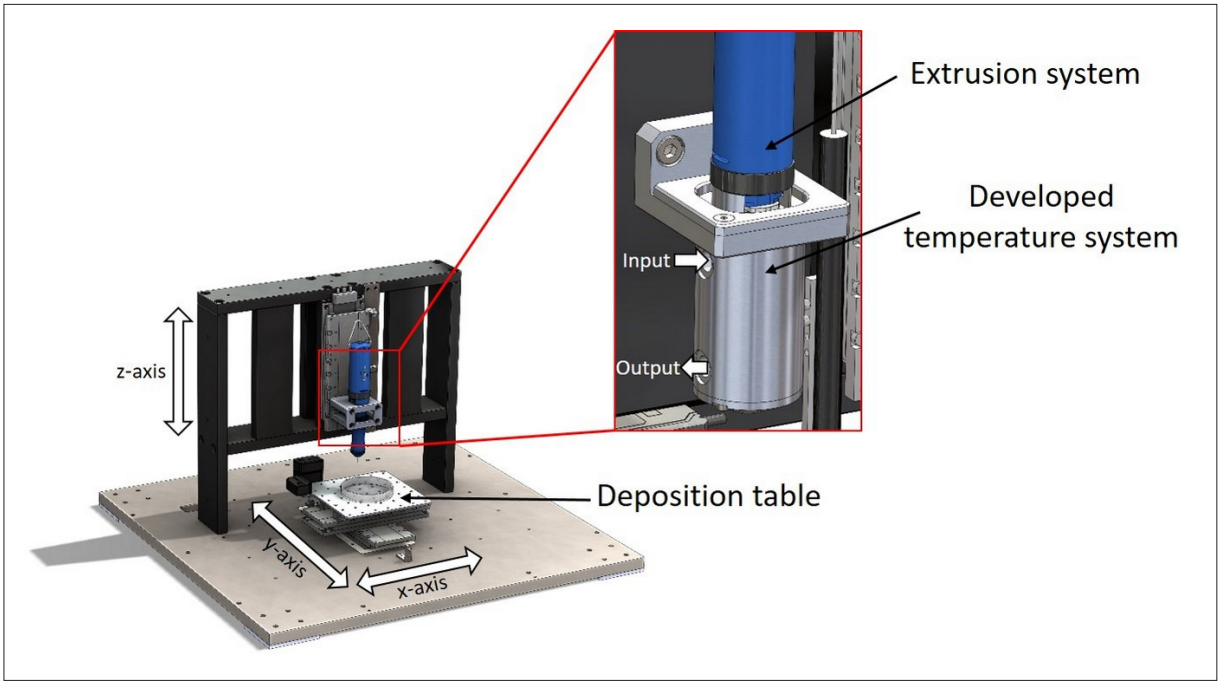

Figure 1. Custom-made bioprinter. The bioprinter is based on three linear axes (x, y, and z) with a micrometer resolution. The extrusion-based machine is under pneumatic control. The bioprinter integrates two temperature systems (head of the syringe and deposition table) composed of an input and output flow, which enables viscosity control of the bioink. The tempered liquid is driven through a hollow circuit set to the desired temperature.

Table 1. List of primers for gene expression analysis

Name	Forward primer (5'–3')	Reverse primer (5'–3')
GAPDH	TCCTGCCCCACCTCCACCAC	GGGCTCCCTAAGCCCCTCCC
COL1A1	CGTGACGCACGGCCAAGAGG	AGATCTGGCAGGGCACGGGT
COL2A1	CTGCTCATCCAGGGCTCAAA	CTTACCGGTGTGTTTCGTGC

The lambs were euthanized, and IVDs were surgically isolated. The AF and NP tissues were cut into ~ 0.5 × 1 cm fragments and rinsed with phosphate-buffered saline (PBS) containing 2% penicillin/streptomycin solution (P/S; 15070-063; Gibco, USA) at room temperature. The tissue fragments were subjected to three consecutive digestions of 0.05% hyaluronidase (H4272; Sigma Aldrich, USA) in Hanks' Balanced Salt Solution (L0606; Biowest, France) for 15 min at 37°C, 0.2% trypsin (T9935; Sigma Aldrich, USA) in Hanks' Balanced Salt Solution for 30 min at 37°C, and 0.25% collagenase (C5138; Sigma Aldrich, USA) in Dulbecco's Modified Eagle culture medium (DMEM containing glucose [GlutaMAX™] and pyruvate; 31966-021; Gibco, USA), supplemented with 10% fetal bovine serum (FBS; S1810; Dominique Deutscher, France), 1% P/S, and 1% amphotericin B (15290; Gibco, USA) for 15 h at 37°C. The cells were filtered through a 70 µm sieve, centrifuged, and resuspended in culture medium before being plated and incubated at 37°C under 5% CO_2. Cells were amplified in DMEM/10% FBS/1% P/S, passaged at 80%–90% confluence, and re-seeded at around 7000 cells/cm².

2.5. Cell phenotype

The differential expression of collagen type I and II in ovine AF and NP cells was assessed by quantitative reverse transcription polymerase chain reaction (RT-qPCR) and immunohistofluorescence (IF).

For RT-qPCR, AF and NP cells at passage 1 were cultivated to confluence in 6-well plates, and RNA was isolated with a Nucleospin RNA XS kit (740902; Macherey-Nagel, Germany). RT was carried out with a Verso cDNA synthesis kit (AB1453A; Thermo Fisher Scientific, USA) with a 1:3 mix of Anchored Oligo(dT) and Random Hexamers. qPCR was performed with SYBR™ Select Master Mix (4472908; Thermo Fisher Scientific, USA) on a thermocycler CFX96 (Bio-Rad, USA) with the primers. The primer sequences are displayed in Table 1 (n = 3 independent experiments), with GAPDH as the internal control in this study. The expression levels of relative genes were normalized to GAPDH, and the results were calculated as fold changes using the $2^{-\Delta\Delta CT}$ formula.

For immunofluorescence, AF and NP cells at passage 4 were cultivated to confluence in 48-well plates, and the cell layers were fixed with 4% (w/v) paraformaldehyde for 20 min. Cells were permeabilized with 0.5% (v/v) Triton X-100 in PBS for 10 min and incubated for 30 min in blocking solution (1% [w/v] bovine serum albumin and 2% [v/v] normal donkey serum in PBS). Primary antibodies for collagen I (ab138492; Abcam, UK) and collagen II (ab34712; Abcam, UK) were diluted at 3.5 and 4.12 µg/mL in blocking solution, respectively, and incubated on the cells for 1 h. Cells were then incubated with the fluorescent secondary antibody (donkey anti-rabbit Alexa Fluor 488; A32790; Thermo Fisher Scientific, USA) diluted at 4 µg/mL in PBS for 1 h, followed by 30 min incubation with Alexa Fluor-568 Phalloidin (A12380; Thermo Fisher Scientific, USA) diluted at 2.5 µg/mL in PBS of and 10 min incubation with DAPI (D1306; Thermo Fisher Scientific, USA) diluted at 2.5 µg/mL in PBS. Image acquisition was performed with a microscope Axio Zoom.V16 (Zeiss, Germany).

2.6. Fluorescent labeling of disc cells

Confluent NP and AF were rinsed with PBS before labeling their cell membrane with fluorochromes. The AF cells were incubated in PBS solution containing 2 µg/mL of 3,3'-dioctadecyl-5,5'-di(4-sulfo-phenyl)oxacarbocyanine, sodium salt (D7778; Sigma Aldrich, USA). NP cells were incubated in a PBS solution containing 2 µg/mL of Vybrant™ CM-DiI Cell-Labeling Solution (V22888; Sigma Aldrich, USA). Both cell types were incubated for 15 min at 37 °C under 5% CO_2, followed by 15 min at 4 °C. A confocal fluorescence microscope (Eclipse Ti2; Nikon, Japan) was used to confirm the fluorescent cell labeling before trypsinizing and mixing cells with the ink.

2.7. Extrusion process

The selected ink composed of 7% (w/v) gelatin, 0.6% (w/v) of alginate, and 0.2% (w/v) of HA was mixed with 2×10^5 cells/mL of either AF cells or NP cells. Syringes were loaded as described above and placed in a nozzle connected to a cooling system set at 22°C. The extrusion was performed through a 0.25 mm diameter needle (7018333; Nordson, USA) into a 100 mm diameter culture dish (430167; Corning, USA). The model was designed based on collagen I histological staining of the lumbar IVD of sheep, and its dimensions were 20 (length [L]) × 16 (width [W]) × 2 mm (height [h]). The resulting IVD construct was crosslinked for 15 min at room temperature

with sterile 100 mmol/L $CaCl_2$ (C7902; Sigma Aldrich, USA) in water. The IVD construct was then transferred to a 35 mm diameter culture dish (83.3900; Sarttedt, Germany) containing culture medium supplemented with 10% FBS, 1% P/S, 1% amphotericin B, and 0.17 mmol/L 2-phospho-L-ascorbic acid (49752; Sigma Aldrich, USA). The construct was incubated at 37°C under 5% CO_2. The culture medium was changed twice a week for up to 21 days. IVD constructs were observed before and after crosslinking and after 21 days of culture using a Dino-Lite microscope (AF4515ZTL; Dino-Lite Microscope, Taiwan). The sample's length, width, and height were measured using ImageJ® software (n = 3 independent experiments).

2.8. Cell visualization, density, and distribution

Cell visualization in the bioprinted construct was performed using fluorescently labeled cells. After 21 days of culture, labeled cells were identified in the IVD construct using a confocal fluorescence microscope. Z-stack acquisition (2.0 mm height; 68 stacks) was performed in six Region Of Interest (ROIs), and Z-projection was used to qualitatively analyze global IVD cell distribution on the x- and y-axis. For cell distribution quantification on the z-axis, cells on Z-stack images corresponding to 0.5, 1.0, 1.5, and 2.0 mm height were counted using the analyze-particle plugin for ImageJ® software (n = 3 experimental replicates). Cell density and distribution were then assessed on non-fluorescently labeled IVD constructs using a Live/Dead™ viability/cytotoxicity kit (L3224; Invitrogen, USA) after 1, 7, 14, and 21 days of culture. The culture medium was removed, and the constructs were rinsed with 2 mmol/L $CaCl_2$ diluted in distilled water. The constructs were then incubated in the dark for 1 h at 37°C with 2 µg/mL of calcein-AM, 4 µg/mL of EthD-1, and 2 µg/mL of Hoechst 33342 trihydrochloride (H3569, λ_{ex} = 352 nm and λ_{em} = 461 nm; Life Technologies, USA), all diluted in culture medium. Constructs were rinsed three times with 2 mmol/L $CaCl_2$ diluted in distilled water and added back to the culture medium. Z-stack acquisition (2.0 mm height) was performed using a confocal fluorescence microscope. Cell density was quantified by counting the number of cells positive to calcein in the entire Z-stack acquisition using the 3D objects counter in ImageJ® software (n = 3 experimental replicates).

2.9. Histological analysis

The IVD constructs were gently removed from the culture dish using a spatula, and excess liquid was removed with a paper towel to limit crystal formation during freezing. The bottom of a freezing cassette (03075; Surgipath, USA) was covered with an Optimal Cutting Temperature (OCT) cryogenic embedding medium (LAMB/OCT; Thermo Fisher Scientific, USA). The constructs were deposited in the center of the cassette and covered with OCT before being immersed for 30 s in isopentane (24872.298; VWR, USA), previously cooled in liquid nitrogen. Once frozen, the samples were sectioned at -20°C into 10 µm slices using a cryostat (CryoStar NX70®; Thermo Fisher Scientific, USA). The slices were then placed on polysine-coated slides (10219280; Thermo Fisher Scientific, USA), and the slides were dried at room temperature for 20 min. Before staining, the samples were post-fixed for 10 min in 4% (w/v) paraformaldehyde to promote the adhesion of the sections onto the slides. Sections were stained following standard protocols with hematoxylin-eosin-saffron (HES; 01562E; Diapath, ITALY) or Alcian blue (AB; 361186; VWR, USA).

2.10. Immunohistochemistry

Enzyme unmasking was performed on post-fixed sections with 0.1% trypsin (T9935; Sigma, USA) in PBS at 37°C for 1 h. Sections were rinsed with PBS and incubated with a 3% solution of H_2O_2 (H1009; Sigma, USA) in PBS at room temperature for 20 min to reduce the non-specific background due to the endogenous peroxidase. Sections were washed with PBS and incubated with 4% bovine serum albumin (A9647; Sigma, USA) and 10% goat serum (G9023; Sigma, USA) in PBS at room temperature for 20 min. The sample sections were then incubated with primary collagen type I antibody (Ab138492; Abcam, UK) diluted at 3.5 µg/mL in antibody diluent (S3022; DAKO, Denmark) overnight at 4°C; negative controls were incubated with only antibody diluent. After a rinsing step with PBS, the sections were incubated for 30 min at room temperature with an anti-rabbit IgG (ImmPRESS HRP Reagent Kit, MP7401; Vector Laboratories, USA). After a rinsing step in PBS, a freshly prepared chromogen 3,3'-diaminobenzidine (SK-4105; ImmPACT, Vector Laboratories, USA) solution was added to the sections. The sections were counterstained with Mayer's hematoxylin and mounted using a permanent aqueous mounting medium (Scy Tek Laboratories, USA); sections were scanned using a microscope slide scanner (NanoZoomer S360; Leica, Germany).

2.11. Statistical analysis

All quantitative data are expressed as the mean ± standard deviation (SD). The statistical analysis comprised paired t-test (gene expression); two-way analysis of variance (ANOVA), followed by Tukey multiple comparisons (parameters for printing conditions, measure of IVD construct size, and z-axis cell distribution); and Shapiro-Wilk test for validating their normality, followed by Tukey comparison test. The analysis was performed using GraphPad Prism version 10.0.0 for Windows (GraphPad Software, USA). A p-value < 0.05 was considered significant.

3. Results

3.1. Optimizing the ink formulation

The first step of the study was to define the concentrations of alginate, gelatin, and HA that would compose the ink (Table 2). First, we selected a gelatin concentration of 8% (w/v) in all inks. We used alginate at 0.6% (w/v) in formulation 1, 1.2% (w/v) in formulation 2, and 1.8% (w/v) in formulation 3. For these three formulations, the ink was granular, and the extruded filaments were not continuous or uniform (Figure S1, Supporting Information). We then added HA to the gelatin/alginate composition to create formulations 4–9, reducing the gelatin concentration to 7% [w/v] to achieve a homogeneous ink and enhance the extrusion process. We noticed that with 0.3% (w/v) of HA, the extruded filaments were continuous but not uniform (formulations 6 and 9). By decreasing the percentage of HA to 0.2% (w/v), the drawn filaments were more uniform (formulations 5 and 8). The formulation that formed a smooth and extrusion-compatible ink with uniform filaments contained 7% (w/v) of gelatin, 0.6% (w/v) of alginate, and 0.2% (w/v) of HA (formulation 5). This formulation was then selected for all subsequent experiments.

3.3. Optimizing the printing conditions

We tested several parameters known to influence the bioprinting process. Different extrusion pressures (70, 90, and 110 kPa), printing speeds (4, 8, and 10 mm/s), and nozzles (stainless steel needle and polyethylene cone of 0.20 and 0.25 mm diameter) were evaluated (Figure 2). Overall, the width of the filament obtained with a 0.20-mm diameter nozzle was significantly lower than that obtained with a 0.25-mm diameter nozzle. For both nozzle types, the filament width was the highest for the highest pressure (110 kPa) or the slowest printing speed (4 mm/s). The filament width increased for a given printing speed and increasing pressure; this increase was more significant with the nozzle of 0.25 mm diameter ($p < 0.01$). In contrast, for a given pressure and increasing printing speed, the filament width decreased for both nozzle modes. Similarly, this decrease was more significant for a nozzle of 0.2 mm ($p < 0.0001$). These differences indicated that the printing speed and pressure affected the bioprinting process. Based on these results, all subsequent experiments were performed using a 0.25-mm diameter needle, a pressure of 70 kPa, and a printing speed of 10 mm/s, which produced filaments with a width of 0.64 ± 0.11 mm.

3.4. Workflow from histological section to bioprinted intervertebral disc construct

After determining the optimal printing parameters, we designed the model to replicate an IVD from a sheep as accurately as possible. First, the phenotype of cells extracted from ovine IVDs was characterized. We used RT-qPCR to confirm that cells isolated from the AF and the NP exhibited distinct gene expression profiles (Figure S2A, Supporting Information). AF cells preferentially expressed COL1A1, while NP cells preferentially expressed COL2A1, as confirmed by immunofluorescence (Figures S2B and S2C, Supporting Information). We then used an IVD of a healthy sheep for the design (Figure 3A). The histological section of the IVD (Figure 3B) was used to generate a virtual 3D model (Figure 3C). We sliced and translated the IVD CAD into G-code instructions (Figure 3D) for further bioprinting using the optimized extrusion parameters (Figure 3E). We then bioprinted

Table 2. Optimization of the ink formulation

Formulation	Concentration (% [w/v])			Ink observation	Extrusion	Filament uniformity
	Alginate	Gelatin	Hyaluronic acid			
F1	0.6	8	-	Granular	Not continuous	N.A.
F2	1.2	8	-	Granular	Not continuous	N.A.
F3	1.8	8	-	Granular	Not continuous	N.A.
F4	0.6	7	-	Homogeneous	Continuous	++
F5	0.6	7	0.2	Homogeneous	Continuous	+++
F6	0.6	7	0.3	Homogeneous	Continuous	+
F7	1.2	7	-	Homogeneous	Continuous	++
F8	1.2	7	0.2	Homogeneous	Continuous	++
F9	1.2	7	0.3	Homogeneous	Continuous	+

Note: Nine formulations of different concentrations (w/v) of alginate, gelatin, and hyaluronic acid were extruded through different needle diameters (0.20 and 0.25 mm) at 20 kPa and with a printing speed of 10 mm/s. The ink aspect (granular or homogeneous), the extrusion process (continuous or not), and the filament uniformity (ranging from + [irregular] to +++ [uniform]) were visually assessed to validate the ink formulation. Abbreviation: N.A., not applicable.

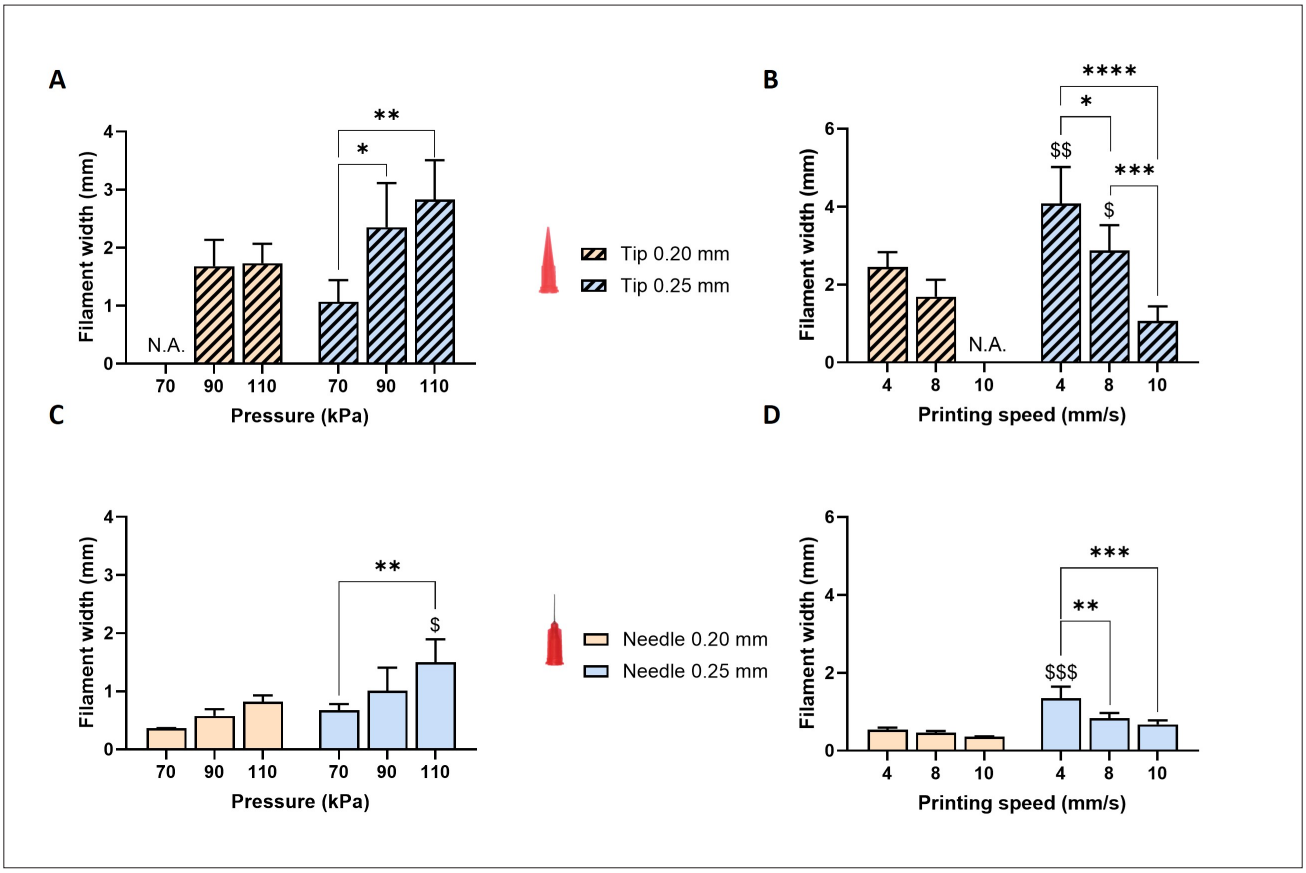

Figure 2. Optimization of printing conditions. (A) Filament width as a function of pressure (printing speed = 10 mm/s) for a tip with different internal diameters (0.20 mm or 0.25 mm). (B) Filament width as a function of printing speed (pressure = 70 kPa) for a tip with different internal diameters (0.20 mm or 0.25 mm). (C) Filament width as a function of pressure (printing speed = 10 mm/s) for a needle with different internal diameters (0.20 mm or 0.25 mm). (D) Filament width as a function of printing speed (pressure = 70 kPa) for a needle with different internal diameters (0.20 mm or 0.25 mm). Bioink comprises 0.6% alginate, 7% gelatin, and 0.2% hyaluronic acid and is extruded at 22°C. Results are expressed as the mean ± standard deviation (n = 3 independent experiments). \$ ($p < 0.05$), \$\$ ($p < 0.01$), \$\$\$ ($p < 0.001$), and \$\$\$\$ ($p < 0.0001$) indicate a significant difference with the 0.20 mm needle or tip at the same pressure or printing speed. *$p < 0.05$; **$p < 0.01$; ***$p < 0.001$; ****$p < 0.0001$ indicate a significant difference. Abbreviation: N.A., not applicable.

the AF section as a multi-lamellar circle, followed by bioprinting of the NP in its center. We crosslinked the resulting IVD construct for 15 min at room temperature with sterile 100 mmol/L $CaCl_2$ in water. We measured the dimensions of the bioprinted constructs immediately after printing, before the crosslinking step, after the crosslinking step, and after 21 days of culture (Figure 3G). The expected dimensions of the construct were 20 (L) × 16 (W) × 2 mm (h). Immediately after printing, the measured dimensions were 21.76 (L) × 17.86 (W) × 2.5 mm (h) and were significantly different from the expected values ($p < 0.05$). After crosslinking, the measured dimensions were 22.65 (L) × 18.45 (W) × 2.53 mm (h). Size measurements were not significantly different from the size before crosslinking, but they were significantly different from the expected values ($p < 0.01$ for the width; $p < 0.001$ for the length). However, after 21 days of culture, we noticed that the construct dimensions decreased to 20.39 (L) × 17.1 (W) × 1.53 mm (h). Even if the length significantly differed after crosslinking ($p < 0.01$), the size was similar to the expected values. The bioprinted structure retained its shape, demonstrating the fidelity of its layout.

3.5. Cell distribution and density

Disc cells (NP and AF cells) were labeled with fluorochromes (Figure 4A) before their incorporation into the ink for bioprinting. Cell distribution in the x-, y-, and z-axes were monitored over 21 days of culture. At day 21, cell membrane labeling was maintained, and NP and AF cells retained their initial distribution within the construct in the x- and y-axis (Figure 4B). The NP (red) and AF (green) cells were observed in the periphery and the center of the construct, respectively.

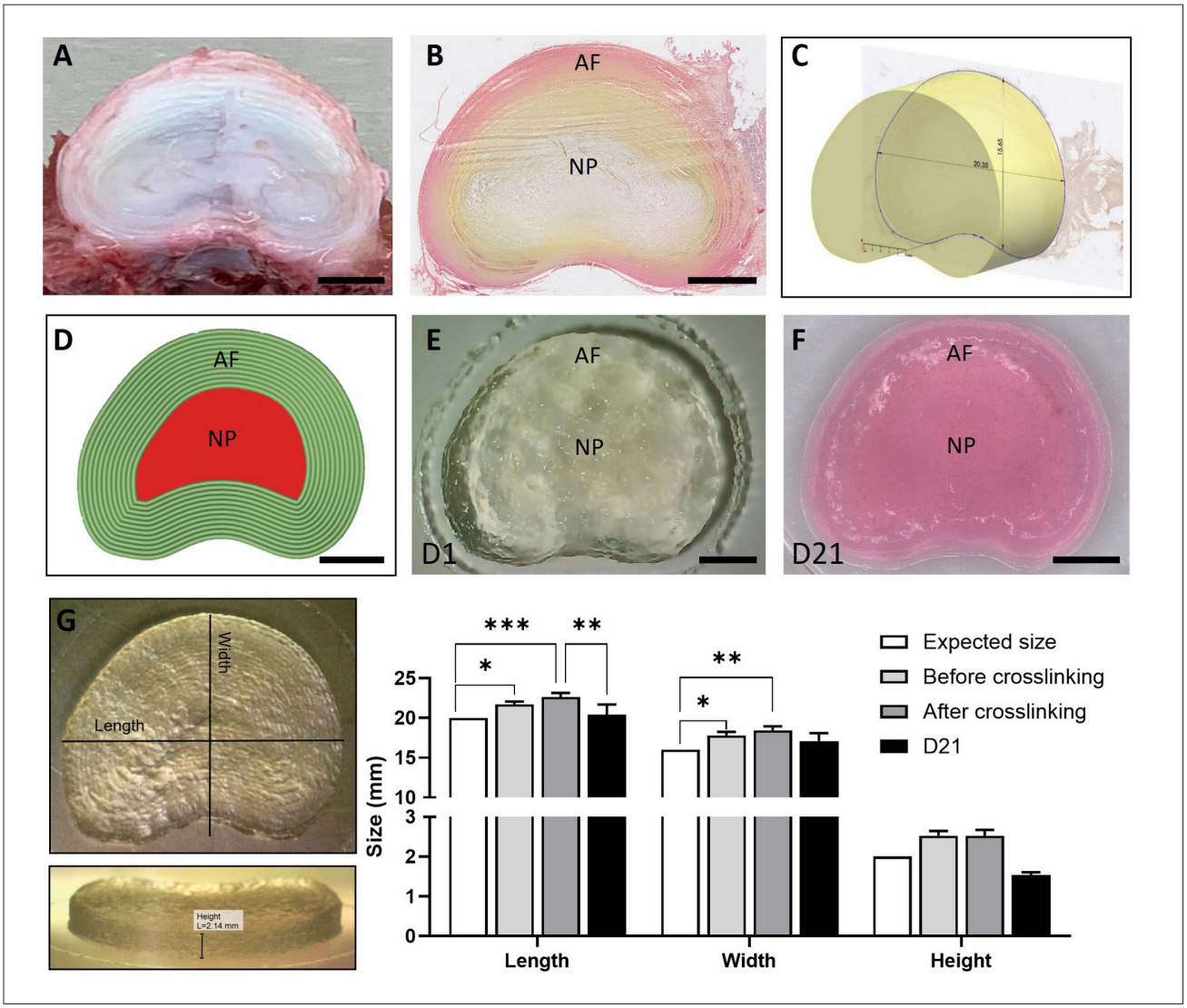

Figure 3. From histological section to bioprinted intervertebral disc (IVD) constructs. (A) The morphological aspect of a lumbar ovine IVD. (B) Collagen I histological staining of an ovine IVD. (C) Virtual 3D model. (D) Slicing 3D IVD model. (E and F) 3D-bioprinted IVD construct after bioprinting (E) and after 21 days of culture (F). (G) Image of the construct and dimensions (length, width, and height) before and after crosslinking and after 21 days at 37°C. The results are expressed as the mean ± standard deviation ($n = 3$ independent experiments). *$p > 0.05$, **$p < 0.01$; ***$p < 0.001$. Scale bars: 5 mm. Abbreviations: AF, annulus fibrosus; NP, *nucleus pulposus*.

Cell distribution on the *z*-axis was also quantified as a function of time (Figures 4C and D and S3, Supporting Information). After 1 day of culture, the NP and AF cells appeared homogenously distributed across the construct height. No differences in the cell number at different heights were observed. In any section of the construct, there were 17–24% NP cells and 19–26% AF cells. After 21 days of culture, the vertical distribution of cells appeared slightly different. The height of the construct decreased from day 1 to day 21. Cells were evident on the top of the constructs at both time points, i.e., 2 mm for day 1 and 1.5 mm for day 21. In contrast, in the lower part of the disk, the percentage of cells increased by 35.6% for NP cells and 33.1% for AF cells at day 21, which is significantly different from day 1 ($p < 0.001$ for NP cells; $p < 0.01$ for AF cells). The final cell density was assessed in the bioprinted IVD construct (Figure 5). Initially, the construct incorporated 1.5×10^5 NP and 1×10^5 AF cells per mL of ink. The AF cell density remained stable for the culture duration, while the NP cell density slightly decreased to 1×10^5 cells/mL after 7 days, then dropped to 2.99×10^4 cells/mL after 21 days of culture.

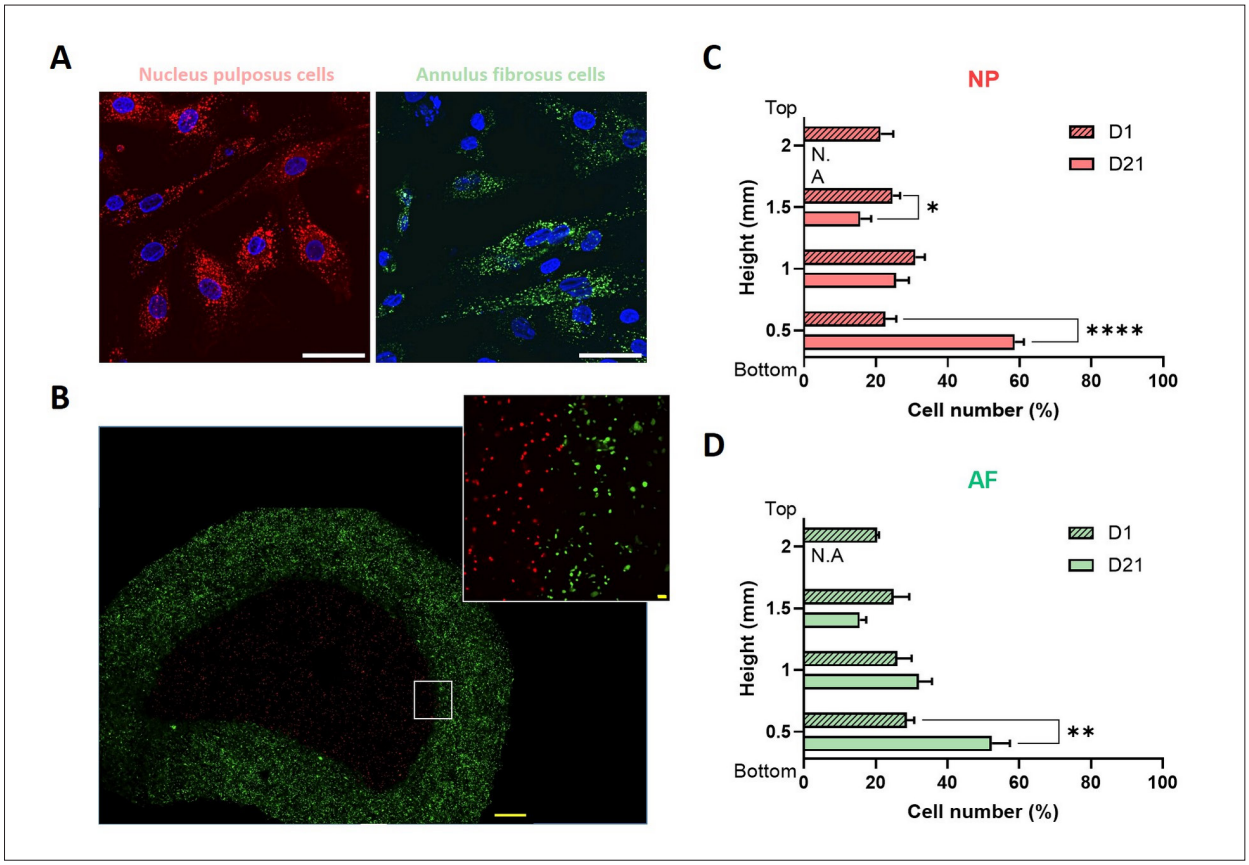

Figure 4. Visualization of fluorescent *nucleus pulposus* (NP) and *annulus fibrosus* (AF) cells and distribution in a bioprinted intervertebral disc (IVD) construct. (A) Representative images of 2D NP cells labeled with Vybrant™ CM-DiI Cell-Labeling Solution (A, left) and 2D AF cells labeled with SP-DiOC18(3) (A, right). (B) IVD fluorescent cells in the IVD construct after 21 days of culture and corresponding zoom-in (B, inset). (C and D) Distribution of NP cells (C) and AF cells (D) in the height of the 3D construct as a function of time (days 1 [D1] and 21 [D21]). Z-stack acquisition (2.0 mm height) was performed in six regions of interest (ROIs). Results are expressed as the mean ± standard deviation (n = 3 experimental replicates). $^{**}p < 0.01$; $^{***}p < 0.001$. Scale bars: 50 µm (A; B, inset); 1 mm (B).

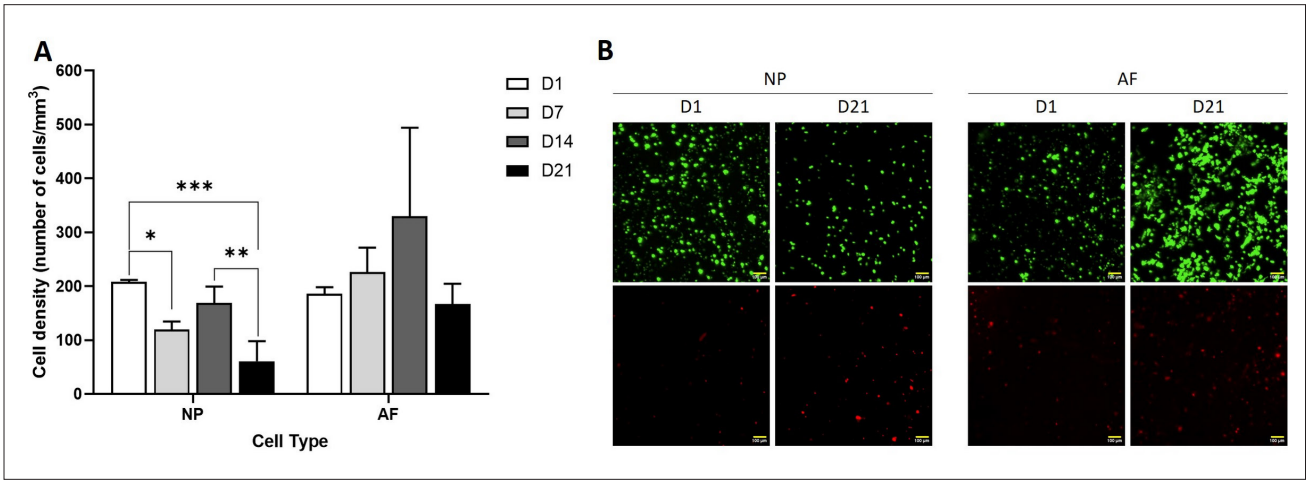

Figure 5. *Nucleus pulposus* (NP) and *annulus fibrosus* (AF) cell density in intervertebral disc (IVD) constructs bioprinted from days 1, 7, 14, and 21 of culture. (A) Cell density (number of cells/mm^3) of both NP and AF parts as a function of time. Results are expressed as the mean ± standard deviation (n = 3 experimental replicates). $^{*}p < 0.05$; $^{**}p < 0.01$; $^{***}p < 0.001$. (B) Representative Z-projection images of cells stained with calcein-AM (green) and ethidium homodimer-1 (red) in the IVD constructs on days 1 and 21. Scale bars: 100 µm.

3.6. Extracellular matrix synthesis and cell morphology

Histological sectioning, staining (HES and AB), and immunohistochemistry (collagen type 1) were performed after 21 days of culture to determine whether the cells printed and cultured in the bioinks synthesized ECM. Sections of a native sheep IVD were also used. AB staining, which highlights the presence of negatively charged molecules, such as polysaccharides, confirmed that after 21 days of culture, the construct was positively stained with AB, highlighting the presence of alginate and HA (Figure 6, top row). Similarly, HES staining indicated the presence of homogenous light pink staining in the AF and NP parts, highlighting the presence of gelatin (Figure 6, middle row). NP and AF cells were identified in the NP and AF sections, respectively. Most cells appeared to be condensed or rounded, and all were positive for intracellular collagen type 1, indicating that the cells were still synthesizing collagen after 21 days of culture (Figures 6, bottom row, and S4, Supporting Information). Sections of a native sheep IVD were also used (Figure S5, Supporting Information).

4. Discussion

Preclinical evaluation of novel biological therapies relies predominantly on studying their efficacy using 2D *in vitro* models. While these models have their uses, particularly in initial studies of cellular toxicity and preliminary proof-of-concept validation, their inability to directly translate results to the *in vivo* environment is a significant constraint. This limitation underscores the urgent need for new *in vitro* models that more accurately represent *in vivo* tissue, thereby improving the translatability of preclinical results to clinical situations. This study, therefore, investigates the possibility of developing a 3D IVD construct containing ovine AF and NP cells, as sheep are widely used as models for disc degeneration. The potential of this new construct to mimic the macroscopic and microscopic organization of the native lumbar ovine IVD promises a more effective approach to preclinical research.

We developed an in-house 3D bioprinter, which we presented here for the first time. It was designed to precisely control the temperature of both the ink used and the printed construct. Owing to the high printing resolution of our printer, the IVD constructs obtained closely matched theoretical models, ensuring high fidelity and precision in their reproduction.

The choice of ink also plays a role in the bioprinting resolution.[46] The selected ink comprises 7% gelatin, 0.6% alginate, and 0.2% HA. It was designed to provide cells with a favorable 3D environment for *de novo* ECM secretion, which, after maturation, forms an IVD-like tissue. Gelatin contributes to the bioink's printability.[47,48] At room temperature, the bioink exhibits the characteristics of an extrudable gel that retains its shape after extrusion when the gelatin concentration is at least 3% (w/v). Furthermore, from a biological point of view, gelatin is obtained by hydrolysis of collagen, which is found in significant quantities in native IVD.[49] Alginate is a

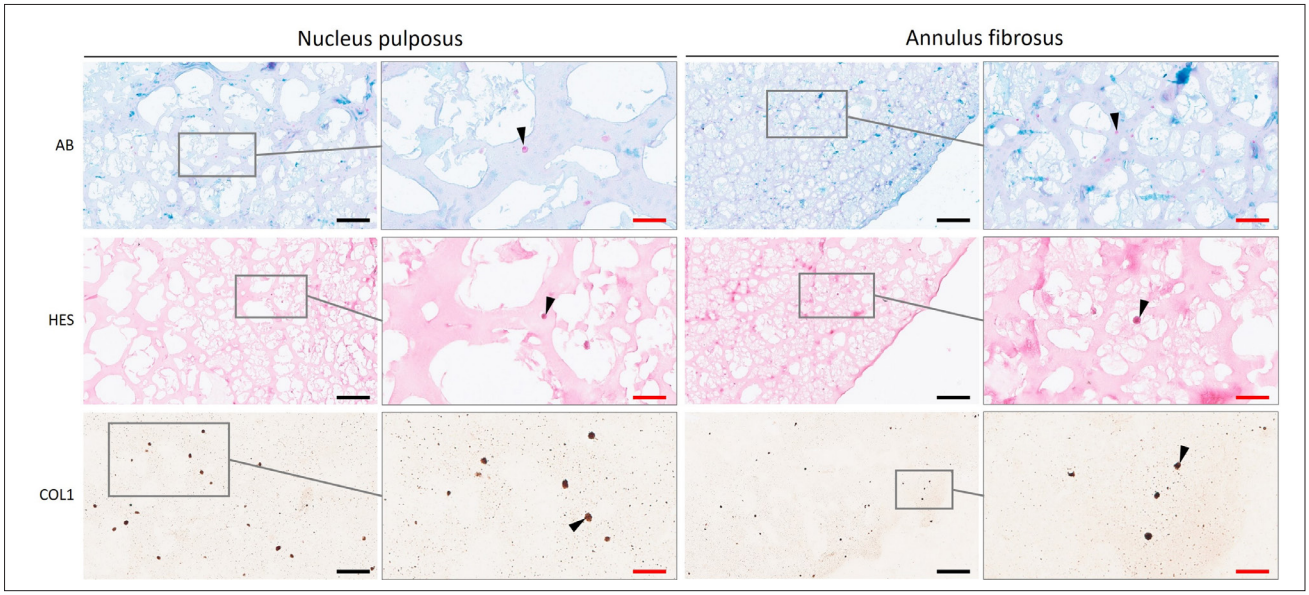

Figure 6. Histological analysis of intervertebral disc (IVD) constructs cultured for 21 days. Representative images of Alcian blue (AB; top row), hematoxylin-eosin-saffron (HES; middle row), and collagen type 1 (COL1; bottom row) staining of *nucleus pulposus* and *annulus fibrosus* parts of the IVD construct after 21 days of culture. Black arrows indicate cells. Scale bars: 200 μm (black); 50 μm (red).

polymer widely used to encapsulate IVD cells and has been reported to promote their specific phenotype.[50,51] After crosslinking with $CaCl_2$, the model was incubated at 37°C. At this temperature, the gelatin liquefies, while the crosslinked alginate retains the 3D structure of the tissue. Finally, HA, a glycosaminoglycan highly present in the NP, is essential in retaining water in the gelatinous body and enhancing the bioink's ability to mimic the IVD. The development of this bioink has also demonstrated that the incorporation of HA enhances its fluidity, thereby facilitating the creation of a deposit filament with superior resolution.[52] The printing conditions of this bioink were then optimized to ensure the highest resolutions. The effect of various parameters, such as nozzle type, pressure, and printing speed on filament size was studied. As expected, the filament is thinner when printing speed increases and pressure decreases. Extrusion pressure has a direct effect on flow and filament thickness. For identical printing speeds, lower pressure reduces the force required to extrude the ink through the nozzle, reducing flow, and filament diameter.[53] Nozzle diameter and geometry also influence filament thickness. Smaller diameter nozzles require higher pressure to maintain the same flow rate as larger diameter nozzles. Consequently, reducing pressure with a smaller nozzle results in a thinner filament due to the lower velocity.[54] Finally, shear stresses are distributed more gradually in tips than in needles, where the transition is rougher. This can lead to thicker filaments with tips, as the bioink undergoes less constriction and shear stress than with needles. Computational fluid dynamics have demonstrated that changes in the design of the nozzle, like the convergence angle and the length of the nozzle, affect the flow rate and shear stress, consequently changing the thickness of the filament.[54,55] The needle was selected in this work because it produces finer filaments compared to the tip. Although the 0.20 mm needle produced finer filaments than the 0.25 mm needle, we did not select it because small diameters increase shear stress, which can damage the cells and reduce their viability and pressure.[55] To minimize the impact of the bioprinting process on the cells, we selected the 0.25 mm needle, the lowest pressure of 70 kPa, and the printing speed of 10 mm/s, which enabled us to obtain the finest filament.

The bioprinted IVD construct was cellularized with cells extracted from a sheep IVD. The sheep model is an *in vivo* model commonly used to study the development of new therapies to treat disc degeneration because of its physiological and anatomical similarities with humans.[56,57] Cell viability was well-maintained in the construct, given the biocompatibility of the ink components. Previous studies using similar inks based on alginate, HA, and gelatin have demonstrated their ability to maintain cell density and viability.[58–60] However, cell density decreased after 21 days in this study, particularly in the NP, further deviating from the *in vivo* cell density of the model. This decrease can be attributed to limited diffusion of the culture medium in the large construct, leading to nutrient and oxygen deficiency in the central regions. This phenomenon of limited diffusion is widely described in the literature, and mathematical models of nutrient diffusion, cell proliferation, and cell death have been investigated.[61] They emphasize a risk for oxygen and glucose depletion within bioprinted constructs, particularly in large ones. In native tissues, a vascular network in the cartilage endplates enables nutrient supply to non-vascularized NP tissues.

The microscopic organization of the IVD was well-reproduced, with the NP cells in the center and the AF cells arranged around them. This organization was maintained throughout the 21-day culture. However, one of the limitations of this work is that this difference between NP and AF was well-marked, whereas, in native IVD, a cellular gradient is observed.[23,62] Indeed, NP cells are more densely populated in the center, and AF cells exhibit a gradual transition in composition and concentration towards the periphery. Incorporating a gradient into the construct could undoubtedly improve the biomimicry of the model by positively influencing cell–cell interactions, thus leading to biological responses closer to those observed in native IVD tissues. Moreover, histological results demonstrated that AF cells, which are elongated *in vivo*, maintained a circular phenotype, as expected in a non-degradable alginate gel. In the bioink, gelatin and HA can support cell adhesion and growth. However, these polymers are soluble because they are not cross-linked, and their persistence over time in the model is uncertain. As a result, the 3D environment is mainly based on alginate, which has no binding sites to which cells can adhere.[63] To improve cell adhesion, the bioink could be enhanced by incorporating a modified alginate with an RGD peptide sequence.[50,51] This sequence serves as a recognition site, allowing AF cells to anchor and acquire a fibroblastic phenotype close to that *in vivo*. Moreover, AF cells did not exhibit any specific organization in the construct. *In vivo*, these cells are aligned along the collagen fibers they produce, which is not the case here. Thus, incorporating a fibrous mesh in the construct also offers significant potential to improve this organization and the model's biomechanical functions.[66–68]

Finally, collagen deposition was not observed, even though the cells expressed the gene associated with collagen production, and intracellular collagen synthesis was demonstrated before and after cell encapsulation. The culture duration might have been too short to allow visible collagen accumulation. Alternatively, the porosity and composition of the microenvironment

could have favored the diffusion of the secreted collagen toward the culture medium, preventing its localized deposition. A longer culture duration might be necessary to allow significant collagen deposition; modifications to the ink composition could also be considered to trap macromolecules synthesized by the cells. Moreover, AF cells are mechanosensitive, meaning they can detect and convert mechanical signals into biochemical signals, such as ECM synthesis. Thus, applying mechanical load to the 3D construct in the future could enhance ECM deposition. Mordechai et al.[69] designed AF laminates made of silk fibers reinforced with alginate hydrogel to replicate native AF mechanical behavior, without the need for collagen synthesis. Moxon et al.[70] reported another approach to mimic the structural properties of an IVD. They printed collagen filaments to stimulate the formation of elongated, mature fibers by the AF cells.[70]

Future studies are warranted to address the shortcomings of this work. Besides incorporating a fibrous mesh to improve the AF organization, using a pre-crosslinked alginate with better stress relaxation properties might favor the deposition of collagen and other ECM molecules, thus enhancing the formation of an IVD-like microenvironment. The next step of this study, which will be crucial to demonstrate the relevance of our work, will be to implement a validation of a therapy's efficacy in the 3D-bioprinted model and in a relevant and well-established preclinical model, such as the sheep, where spontaneous disc degeneration occurs. Once the relevance of this type of bioprinted model has been validated, the incorporation of primary human NP and AF cells, although scarcely available, could be implemented to demonstrate the ability of a bioprinted IVD model in accurately predicting the success of bioinspired therapies for IVD degeneration.

5. Conclusion

In this study, we demonstrated the potential of bioprinting technology to fabricate a 3D model that mimics the architecture of a native IVD. Using an in-house extrusion bioprinter, we optimized bioprinting parameters (filament width, pressure, printing speed, and nozzle type) and the 3D cellular organization. We displayed the structural similarity and the excellent integration of both AF and NP tissues, thereby highlighting the promising potential of this IVD construct in the development of relevant *in vitro* models.

Acknowledgments

The authors acknowledge the SC3M platform from the INSERM/NU/ONIRIS UMR1229 RMeS Laboratory (SFR Bonamy, BioCore, Inserm UMS 016, CNRS UAR 3556, Nantes, France) and the IBISA MicroPICell facility (Biogenouest, France), a member of the national infrastructure France-Bioimaging, supported by the French National Research Agency (ANR-10-INBS-04). The authors thank Hilel Moussi for their assistance. The graphical abstract was created using BioRender.

Funding

This study was supported by the RFI Bioregate program of Pays de la Loire Region within the framework of the 4D-BIODIV project, the European Commission's Horizon 2020 funding program for the iPSpine project (grant number: 825925), the EXCELLDISC project (ANR-19-CE18-0020-01), and the INDEED project (ANR-19-CE06-0028-02).

Conflict of interest

The authors declare they have no competing interests.

Author contributions

Conceptualization: J.Y. Hascoët, J. Guicheux, C. Le Visage, J. Clouet, M. Fusellier, V. Delplace, P. Weiss, F. Halary
Formal analysis: E. Carrot, P. de Villemagne, L. Vidal
Funding acquisition: J.Y. Hascoët, J. Guicheux, C. Le Visage
Investigation: E. Carrot, P. de Villemagne, P. Humbert, S. Grastilleur, B. Rosa, B. Halgand, Y. Le Guennec
Methodology: E. Carrot, P. Humbert, S. Grastilleur
Writing–original draft: E. Carrot, C. Le Visage
Writing–review & editing: All authors

Ethics approval and consent to participate

Not applicable.

Consent for publication

Not applicable.

Availability of data

Data used in this work are available from the corresponding author upon reasonable request.

References

1. Wilke HJ, Galbusera F. Biomechanics of the healthy and diseased spine. In: Biological Approaches to Spinal Disc Repair and Regeneration for Clinicians (1st ed.). Stuttgart, Germany: Georg Thieme Verlag KG; 2017:30-36. doi: 10.1055/b-0037-145106

2. Amin DB, Lawless IM, Sommerfeld D, Stanley RM, Ding B, Costi JJ. The effect of six degree of freedom loading sequence

on the in-vitro compressive properties of human lumbar spine segments. *J Biomech*. 2016;49(14):3407-3414. doi: 10.1016/j.jbiomech.2016.09.009

3. Gravel JT, Abduljabbar FH, Ouellet J, Haglund L. The human spinal disc: relevant anatomy and physiology. In: Biological Approaches to Spinal Disc Repair and Regeneration for Clinicians (1st ed.). Stuttgart, Germany: Georg Thieme Verlag KG; 2017:2-10. doi: 10.1055/b-0037-145103
4. Lavignolle B. The intervertebral disc. In: Vital JM, Cawley DT, eds. *Spinal Anatomy : Modern Concepts*. Springer International Publishing; 2020:207-216. doi: 10.1007/978-3-030-20925-4_14
5. Al-Abbasi M, Al-Rubai AJF, Assi MH. Quantification of the water content of human intervertebral discs in various regions and conditions. *Al-Rafidain J Med Sci*. 2024;6(2):43-47. doi: 10.54133/ajms.v6i2.715
6. Johnstone B, Bayliss MT. The large proteoglycans of the human intervertebral disc. Changes in their biosynthesis and structure with age, topography, and pathology. *Spine*. 1995;20(6):674-684. doi: 10.1097/00007632-199503150-00008
7. Pattappa G, Li Z, Peroglio M, Wismer N, Alini M, Grad S. Diversity of intervertebral disc cells: phenotype and function: diversity of intervertebral disc cells. *J Anat*. 2012;221(6):480-496. doi: 10.1111/j.1469-7580.2012.01521.x
8. Sivan SS, Hayes AJ, Wachtel E, et al. Biochemical composition and turnover of the extracellular matrix of the normal and degenerate intervertebral disc. *Eur Spine J*. 2014;23 (Suppl. 3):S344-S353. doi: 10.1007/s00586-013-2767-8
9. Zhang S, Liu W, Chen S, et al. Extracellular matrix in intervertebral disc: basic and translational implications. *Cell Tissue Res*. 2022;390(1):1-22. doi: 10.1007/s00441-022-03662-5
10. Vogel A, Pioletti DP. Damping properties of the nucleus pulposus. *Clin Biomech*. 2012;27(9):861-865. doi: 10.1016/j.clinbiomech.2012.06.005
11. Krull C, Lutton A, Olesik J, Walter B. A method for measuring intra-tissue swelling pressure using a needle micro-osmometer. *Eur Cell Mater*. 2020;40:146-159. doi: 10.22203/eCM.v040a09
12. Urban JPG, McMullin JF. Swelling pressure of the inervertebral disc: influence of proteoglycan and collagen contents. *Biorheology*. 1985;22(2):145-157. doi: 10.3233/BIR-1985-22205
13. Pazzaglia UE, Salisbury JR, Byers PD. Development and involution of the Notochord in the human spine. *J R Soc Med*. 1989;82(7):413-415. doi: 10.1177/014107688908200714
14. Tan Z, Chen P, Dong X, et al. Progenitor-like cells contributing to cellular heterogeneity in the nucleus pulposus are lost in intervertebral disc degeneration. *Cell Rep*. 2024;43(6):114342. doi: 10.1016/j.celrep.2024.114342
15. Risbud MV, Schoepflin ZR, Mwale F, et al. Defining the phenotype of young healthy nucleus pulposus cells: recommendations of the Spine Research Interest Group at the 2014 annual ORS meeting. *J Orthop Res*. 2015;33(3):283-293. doi: 10.1002/jor.22789
16. Mwale F, Roughley P, Antoniou J. Distinction between the extracellular matrix of the nucleus pulposus and hyaline cartilage: a requisite for tissue engineering of intervertebral disc. *Eur Cells A¨nd Mater*. 2004;8:58-64. doi: 10.22203/eCM.v008a06
17. Tomaszewski KA, Walocha JA, Mizia E, Gładysz T, Głowacki R, Tomaszewska R. Age- and degeneration-related variations in cell density and glycosaminoglycan content in the human cervical intervertebral disc and its endplates. *Pol J Pathol*. 2015;66(3):296-300. doi: 10.5114/pjp.2015.54964
18. Urban JPG, Roberts S, Ralphs JR. The nucleus of the intervertebral disc from development to degeneration. *Am Zool*. 2000;40(1):53-061. doi: 10.1093/icb/40.1.53
19. Marchand F, Ahmed AM. Investigation of the laminate structure of lumbar disc anulus fibrosus. *Spine*. 1990;15(5):402-410. doi: 10.1097/00007632-199005000-00011
20. Liang H, Luo R, Li G, Zhang W, Song Y, Yang C. The proteolysis of ECM in intervertebral disc degeneration. *Int J Mol Sci*. 2022;23(3):1715. doi: 10.3390/ijms23031715
21. Costi JJ, Stokes IA, Gardner-Morse M, Laible JP, Scoffone HM, Iatridis JC. Direct measurement of intervertebral disc maximum shear strain in six degrees of freedom: motions that place disc tissue at risk of injury. *J Biomech*. 2007;40(11):2457-2466. doi: 10.1016/j.jbiomech.2006.11.006
22. Guerin HAL, Elliott DM. Structure and properties of soft tissues in the spine. In: *Spine Technology Handbook*. Academic Press; 2006:35-62. doi: 10.1016/B978-012369390-7/50004-6
23. Torre OM, Mroz V, Bartelstein MK, Huang AH, Iatridis JC. Annulus fibrosus cell phenotypes in homeostasis and injury: implications for regenerative strategies. *Ann N Y Acad Sci*. 2019;1442(1):61-78. doi: 10.1111/nyas.13964
24. Liebscher T, Haefeli M, Wuertz K, Nerlich AG, Boos N. Age-related variation in cell density of human lumbar intervertebral disc. *Spine*. 2011;36(2):153-159. doi: 10.1097/brs.0b013e3181cd588c
25. Samanta A, Lufkin T, Kraus P. Intervertebral disc degeneration—current therapeutic options and challenges. *Front Public Health*. 2023;11:1156749.

doi: 10.3389/fpubh.2023.1156749

26. Casiano VE, Sarwan G, Dydyk AM, Varacallo M. Back pain. In: *StatPearls*. StatPearls Publishing; 2023. Accessed March 29, 2023. http://www.ncbi.nlm.nih.gov/books/NBK538173/

27. Hay SI, Abajobir AA, Abate KH, et al. Global, regional, and national disability-adjusted life-years (DALYs) for 333 diseases and injuries and healthy life expectancy (HALE) for 195 countries and territories, 1990–2016: a systematic analysis for the Global Burden of Disease Study 2016. *Lancet*. 2017;390(10100):1260-1344. doi: 10.1016/S0140-6736(17)32130-X

28. Meddeba M, Hatirab F, Habboubia K, Mestiria. Biomechanical Study of the Behavior of the Intervertebral Disc: Intact Lumbar Spine Versus Arthrodesis. *J Orthop Bone Disord*. 2024;8(2):1-4. doi: 10.23880/jobd-16000265

29. Sampara P, Banala RR, Vemuri SK, Av GR, Gpv S. Understanding the molecular biology of intervertebral disc degeneration and potential gene therapy strategies for regeneration: a review. *Gene Ther*. 2018;25(2):67-82. doi: 10.1038/s41434-018-0004-0

30. Tamagawa S, Schol J, Sakai D. Cell therapy for intervertebral disc regeneration: progress and hurdles in clinical translation. *Indian Spine J*. 2024;7(2):131-141. doi: 10.4103/isj.isj_17_24

31. Liu Y, Zhao Z, Guo C, et al. Application and development of hydrogel biomaterials for the treatment of intervertebral disc degeneration: a literature review. *Front Cell Dev Biol*. 2023;11:1286223. doi: 10.3389/fcell.2023.1286223

32. Doench I, Tran TA, David L, et al. Cellulose nanofiber-reinforced chitosan hydrogel composites for intervertebral disc tissue repair. *Biomimetics (Basel)*. 2019;4(1):19. doi: 10.3390/biomimetics4010019

33. Hingert D, Barreto Henriksson H, Baranto A, Brisby H. BMP-3 promotes matrix production in co-cultured stem cells and disc cells from low back pain patients. *Tissue Eng Part A*. 2020;26(1-2):47-56. doi: 10.1089/ten.tea.2019.0125

34. Tang SN, Salazar-Puerta AI, Heimann MK, et al. Engineered extracellular vesicle-based gene therapy for the treatment of discogenic back pain. *Biomaterials*. 2024;308:122562. doi: 10.1016/j.biomaterials.2024.122562

35. Barcellona MN, Ní Néill T, O'Brien FJ, Dixon JE, Curtin CM, Buckley CT. Modulation of inflammation and regeneration in the intervertebral disc using enhanced cell-penetrating peptides for MicroRNA delivery. *Adv NanoBiomed Res*. 2024;4(7):2300112. doi: 10.1002/anbr.202300112

36. Yuan B, Rudeen K, Li J, et al. Biodegradable microspheres and hydrogel drug delivery system of tumor necrosis factor (TNF) inhibitor and growth differentiation factor 5 (GDF5) reduces disk inflammation in the rabbit model. *Spine (Phila Pa 1976)*. 2023;48(15):E257-E265. doi: 10.1097/BRS.0000000000004686

37. Rivera Tapia ED, Meakin JR, Holsgrove TP. In-vitro models of disc degeneration – a review of methods and clinical relevance. *J Biomech*. 2022;142:111260. doi: 10.1016/j.jbiomech.2022.111260

38. Yung Lee J, Hall R, Pelinkovic D, et al. New use of a three-dimensional pellet culture system for human intervertebral disc cells: initial characterization and potential use for tissue engineering. *Spine* (Phila Pa 1976). 2001;26(21):2316-2322. doi: 10.1097/00007632-200111010-00005

39. Le Maitre CL, Freemont AJ, Hoyland JA. The role of interleukin-1 in the pathogenesis of human intervertebral disc degeneration. *Arthritis Res Ther*. 2005;7(4):R732. doi: 10.1186/ar1732

40. McDonnell EE, Buckley CT. Two- and three-dimensional in vitro nucleus pulposus cultures: an in silico analysis of local nutrient microenvironments. *JOR Spine*. 2022;5(3):e1222. doi: 10.1002/jsp2.1222

41. Zhang A, Cheng Z, Chen Y, Shi P, Gan W, Zhang Y. Emerging tissue engineering strategies for annulus fibrosus therapy. *Acta Biomater*. 2023;167:1-15. doi: 10.1016/j.actbio.2023.06.012

42. Liu Y, Peng L, Li L, et al. 3D-bioprinted BMSC-laden biomimetic multiphasic scaffolds for efficient repair of osteochondral defects in an osteoarthritic rat model. *Biomaterials*. 2021;279:121216. doi: 10.1016/j.biomaterials.2021.121216

43. Yuan D, Chen Z, Xiang X, et al. The establishment and biological assessment of a whole tissue-engineered intervertebral disc with PBST fibers and a chitosan hydrogel in vitro and in vivo. *J Biomed Mater Res B Appl Biomater*. 2019;107(7):2305-2316. doi: 10.1002/jbm.b.34323

44. Fusellier M, Clouet J, Gauthier O, Tryfonidou M, Le Visage C, Guicheux J. Degenerative lumbar disc disease: in vivo data support the rationale for the selection of appropriate animal models. *Eur Cell Mater*. 2020;39:17-48. doi: 10.22203/eCM.v039a02

45. Pourchet LJ, Thepot A, Albouy M, et al. Human skin 3D bioprinting using scaffold-free approach. *Adv Healthc Mater*. 2017;6(4):1601101. doi: 10.1002/adhm.201601101

46. Wang J, Cui Z, Maniruzzaman M. Bioprinting: a focus on improving bioink printability and cell performance based on different process parameters. *Int J Pharm*. 2023;640:123020. doi: 10.1016/j.ijpharm.2023.123020

47. Abedi K, Keshvari H, Solati-Hashjin M. Extrusion-based bioprinting: considerations toward gelatin-alginate bioink. *Rapid Prototyp J*. 2024;30(6):1094-1104. doi: 10.1108/RPJ-06-2023-0207

48. Seok JM, Ahn M, Kim D, et al. Decellularized matrix bioink with gelatin methacrylate for simultaneous improvements

in printability and biofunctionality. *Int J Biol Macromol*. 2024;262:130194.
doi: 10.1016/j.ijbiomac.2024.130194

49. Rajasekaran S, Soundararajan DCR, Nayagam SM, et al. Novel biomarkers of health and degeneration in human intervertebral discs: in-depth proteomic analysis of collagen framework of fetal, healthy, scoliotic, degenerate, and herniated discs. *Asian Spine J*. 2023;17(1):17-29.
doi: 10.31616/asj.2021.0535

50. Melrose J, Smith S, Ghosh P, Taylor TKF. Differential expression of proteoglycan epitopes and growth characteristics of intervertebral disc cells grown in alginate bead culture. *Cells Tissues Organs*. 2001;168(3):137-146.
doi: 10.1159/000047829

51. Thonar E, An H, Masuda K. Compartmentalization of the matrix formed by nucleus pulposus and annulus fibrosus cells in alginate gel. *Biochem Soc Trans*. 2002;30(6):874-878.
doi: 10.1042/bst0300874

52. Ouyang L, Yao R, Zhao Y, Sun W. Effect of bioink properties on printability and cell viability for 3D bioplotting of embryonic stem cells. *Biofabrication*. 2016;8(3):035020.
doi: 10.1088/1758-5090/8/3/035020

53. Habib MA, Khoda B. Rheological analysis of bio-ink for 3D bio-printing processes. *J Manuf Process*. 2022;76:708-718.
doi: 10.1016/j.jmapro.2022.02.048

54. Magalhães IP, Oliveira PMD, Dernowsek J, Casas EBL, Casas MSL. Investigation of the effect of nozzle design on rheological bioprinting properties using computational fluid dynamics. *Matéria (Rio J.)* 2019;24(3):e12401.
doi: 10.1590/s1517-707620190003.0714

55. Chand R, Muhire BS, Vijayavenkataraman S. Computational fluid dynamics assessment of the effect of bioprinting parameters in extrusion bioprinting. *Int J Bioprint*. 2022; 8(2):545.
doi: 10.18063/ijb.v8i2.545

56. Reitmaier S, Schmidt H. Review article on spine kinematics of quadrupeds and bipeds during walking. *J Biomech*. 2020;102:109631.
doi: 10.1016/j.jbiomech.2020.109631

57. Yoshizato H, Morimoto T, Nonaka T, et al. Animal model for anterior lumbar interbody fusion: a literature review. *Spine Surg Relat Res*. 2024;8(4):373-382.
doi: 10.22603/ssrr.2023-0262

58. Duan B, Hockaday LA, Kang KH, Butcher JT. 3D bioprinting of heterogeneous aortic valve conduits with alginate/gelatin hydrogels. *J Biomed Mater Res A*. 2013;101A(5):1255-1264.
doi: 10.1002/jbm.a.34420

59. Fedorovich NE, De Wijn JR, Verbout AJ, Alblas J, Dhert WJA. Three-dimensional fiber deposition of cell-laden, viable, patterned constructs for bone tissue printing. *Tissue Eng Part A*. 2008;14(1):127-133.
doi: 10.1089/ten.a.2007.0158

60. Wang X, Yan Y, Pan Y, et al. Generation of three-dimensional hepatocyte/gelatin structures with rapid prototyping system. *Tissue Eng*. 2006;12(1):83-90.
doi: 10.1089/ten.2006.12.83

61. Gironi P, Petraro L, Santoni S, Dedé L, Colosimo BM. A computational model of cell viability and proliferation of extrusion-based 3D-bioprinted constructs during tissue maturation process. *Int J Bioprinting*. 2023;9(4):741.
doi: 10.18063/ijb.741

62. Bruehlmann SB, Rattner JB, Matyas JR, Duncan NA. Regional variations in the cellular matrix of the annulus fibrosus of the intervertebral disc. *J Anat*. 2002;201(2):159-171.
doi: 10.1046/j.1469-7580.2002.00080.x.

63. Rastogi P, Kandasubramanian B. Review of alginate-based hydrogel bioprinting for application in tissue engineering. *Biofabrication*. 2019;11(4):042001.
doi: 10.1088/1758-5090/ab331e

64. Li QQ, Xu D, Dong QW, Song XJ, Chen YB, Cui YL. Biomedical potentials of alginate via physical, chemical, and biological modifications. *Int J Biol Macromol*. 2024; 277:134409.
doi: 10.1016/j.ijbiomac.2024.134409

65. Sandvig I, Karstensen K, Rokstad AM, et al. RGD-peptide modified alginate by a chemoenzymatic strategy for tissue engineering applications. *J Biomed Mater Res A*. 2015; 103(3):896-906.
doi: 10.1002/jbm.a.35230

66. Yang J, Yang X, Wang L, et al. Biomimetic nanofibers can construct effective tissue-engineered intervertebral discs for therapeutic implantation. *Nanoscale*. 2017;9(35):13095-13103.
doi: 10.1039/c7nr03944a

67. Zhou P, Chu G, Yuan Z, et al. Regulation of differentiation of annulus fibrosus-derived stem cells using heterogeneous electrospun fibrous scaffolds. *J Orthop Transl*. 2021;26: 171-180.
doi: 10.1016/j.jot.2020.02.003

68. Gluais M, Clouet J, Fusellier M, et al. In vitro and in vivo evaluation of an electrospun-aligned microfibrous implant for Annulus fibrosus repair. *Biomaterials*. 2019;205:81-93.
doi: 10.1016/j.biomaterials.2019.03.010

69. Mordechai HS, Aharonov A, Sharon SE, et al. Toward a mechanically biocompatible intervertebral disc: engineering of combined biomimetic annulus fibrosus and nucleus pulposus analogs. *J Biomed Mater Res A*. 2023;111(5):618-633.
doi: 10.1002/jbm.a.37519

70. Moxon SR, McMurran Z, Kibble MJ, Domingos M, Gough JE, Richardson SM. 3D bioprinting of an intervertebral disc tissue analogue with a highly aligned annulus fibrosus via suspended layer additive manufacture. *Biofabrication*. 2024;17(1):015005.
doi: 10.1088/1758-5090/ad8379